J. Fluid Mech. (1976), *vol.* 78, *part* 2, *pp.* 217–235
Printed in Great Britain

On spatially growing baroclinic waves in the ocean

By NELSON G. HOGG

Woods Hole Oceanographic Institution, Woods Hole, Massachusetts 02543

(Received 28 July 1975 and in revised form 20 May 1976)

It is shown that spatially growing waves with complex wavenumber and real frequency can exist in a baroclinic flow and that these waves are substantially different from the more commonly studied temporally growing ones. They are bounded by a *low* wavenumber cut-off which separates them from the temporally growing waves. Their amplitude and phase change most rapidly near their steering level and are almost depth independent away from it. Most of the energy conversion from mean flow to the waves occurs at this level. It is suggested that these motions may be forced by steady disturbances such as bottom relief.

The theory is compared with recent observations of strong small-scale motions in a region of rough topography of MODE and in the vicinity of the Gulf Stream. The vertical structure can be well matched with the theory but the complex wavenumber appears to be a factor of 2–3 greater than that predicted.

1. Introduction

It was first demonstrated by Charney (1947) and Eady (1949) that the potential energy stored in the general circulation of the atmosphere and oceans could be transferred into smaller-scale fluctuations through a process that has come to be known as 'baroclinic instability'. Since this pioneering work, much has been learned about the dependence of the fluctuation properties on various parameters. Most recently, Gill, Green & Simmons (1974) have carefully analysed situations relevant to oceanography.

The main thrust of these studies has been to assume that the basic flow is horizontally uniform and that the perturbations have separable vertical dependence and wavelike lateral and temporal behaviour. Application of suitable boundary conditions at the surface and bottom gives rise to a vertical eigenvalue problem for the complex phase speed c as a function of the wavenumber k.

Choosing k to be real one searches for roots for which $c_i > 0$ so that an exponential growth rate of kc_i results. These waves are, therefore, unstable. In general, however, c is an analytic function of the *complex* wavenumber k. Charney & Stern (1962) and Lin (1955) have pointed out the close analogy between stability problems for baroclinic shear flow and the more extensively analysed homogeneous non-rotating shear flow. In the latter, it has been recognized (Watson 1962; Gaster 1962, 1965*a*, *b*) that the complementary situation of complex k and real frequency $\omega = kc$ is more applicable to laboratory demonstrations of instability. Here, typically, a disturbance is introduced using some kind of vibrating wavemaker with real frequency and instabilities with spatial growth are observed.

The analyses with real wavenumber are clearly of value and would seem, intuitively, to apply to the spontaneous instability of a baroclinic current owing to, say, an initial disturbance with real wavenumber. However, consider the following situation. A wave maker sits on the bottom of the ocean vibrating with real frequency ω. Clearly this will force waves with a similar real frequency and these will propagate in the direction of their group velocity. If the eigenvalue problem (alternatively the dispersion relation $c(k)$) permits a negative imaginary part for k (and the group velocity is positive), these waves will grow in their direction of propagation. As the wave-maker frequency tends to zero we approach the disturbance that would be produced by a stationary object such as bottom topography. This argument is similar in vein to Lighthill's (1967) work on travelling forcing effects. In § 2 we shall outline the theoretical concepts and show that spatially growing waves are possible, although we shall not solve the full problem outlined above.

In the case of homogeneous shear flow, Gaster (1962, 1965*a*, *b*) has shown that the transformation from spatially growing waves with a wavenumber of given real part to temporally growing waves with the same wavenumber is particularly simple under certain circumstances and just involves the group velocity. The main requirement is that the growth rate is small. However, the baroclinic situation is decidedly different. We find in § 3 that spatial and temporal waves are separated in wavenumber with short waves being spatially unstable and long waves being temporally unstable. A neutral wave separates the two cases. We also display modal amplitudes as functions of depth and show that these are substantially different for the two cases.

This study is carried out for a particularly simple case in which the basic flow is the first baroclinic mode. Two kinds of stratification are considered: a uniform and an exponential function of depth. The top and bottom boundaries are taken to be rigid and horizontal and the rotation rate to be uniform. This implies that the top and bottom surfaces are isopycnals and vortex stretching takes place in the interior because the isopycnal slope is a function of depth.

In § 4 we present, briefly, observational work by Tom Sanford and John Swallow from the MODE experiment that originally inspired this investigation. We also show some measurements by Peter Saunders and Jim Luyten from the Gulf Stream which appear to support application of this work to the real world.

2. Fundamentals

If we define $\mathbf{u}(\mathbf{x}, t) \equiv (u, v, w)$, $p(\mathbf{x}, t)$ and $\rho(\mathbf{x}, t)$, functions of position $\mathbf{x} = (x, y, z)$ and time t, as small amplitude disturbances in velocity, pressure and density from the basic-state values of $\overline{U}(z)$, $\overline{P}(y, z)$ and $\overline{\rho}(y, z)$ then the vertical component of relative vorticity $\zeta(\mathbf{x}, t)$ is approximately governed by the equation

$$\frac{d}{dt}\zeta = fw_z, \quad \frac{d}{dt} = \frac{\partial}{\partial t} + \overline{U}(z)\frac{\partial}{\partial x}, \tag{1}$$

in the absence of dissipation and variation in the planetary vorticity $f = 2\Omega \sin \phi_0$ (Ω = earth's rotation rate and ϕ_0 is the central latitude in the region of con-

sideration). We assume that the flow is slow relative to a rapidly rotating earth so that the motion is quasi-geostrophic and hydrostatic. Therefore

$$f\overline{U}(z) = -\overline{P}_y/\rho_0, \quad 0 = -\overline{P}_z - g\overline{\rho} \tag{2}$$

and

$$fu = -p_y/\rho_0, \quad fv = p_x/\rho_0, \quad 0 = -p_z - g\rho, \tag{3}$$

so that the vorticity $\zeta = v_x - u_y = \nabla_h^2 p/\rho_0 f$ (ρ_0 is a constant reference density and g the acceleration of gravity). Density is conserved in the motion; with the Boussinesq approximation this leads to

$$\frac{d}{dt}\rho + \frac{\rho_0 f}{g}\overline{U}_z(z)\, v - \frac{\rho_0 N^2(z)}{g} w = 0, \tag{4}$$

where $N^2(z) = -(g/\rho_0)\,\partial\overline{\rho}/\partial z$ is the Brunt–Väisälä frequency.

Equation (4) can be used to evaluate the stretching term on the right side of (1). Doing so we obtain

$$\frac{d}{dt}\left[\zeta - \frac{gf}{\rho_0}\frac{\partial}{\partial z}\left(\frac{\rho}{N^2}\right)\right] - v\frac{\partial}{\partial z}\left(\frac{f^2\overline{U}_z}{N^2}\right) p_x = 0. \tag{5}$$

Upon substituting for ζ and ρ from the hydrostatic and geostrophic relations (5) becomes

$$\frac{d}{dt}\left[\nabla_h^2 p + \frac{\partial}{\partial z}\left(\frac{f^2}{N^2} p_z\right)\right] - \frac{\partial}{\partial z}\left(\frac{f^2\overline{U}_z}{N^2}\right) p_x = 0. \tag{6}$$

The factor

$$Q_y = -\frac{\partial}{\partial z}\left(\frac{f^2\overline{U}_z}{N^2}\right)$$

is the cross-stream gradient of potential vorticity in the basic flow (inclusion of 'β-effects' for zonal currents leads simply to the addition of β to Q_y).

By choosing two-dimensional periodic disturbances of the form

$$p(\mathbf{x}, t) = F(z)\, e^{ik(x-ct)}, \tag{7}$$

where $F(z)$ is a complex amplitude, c the complex phase speed and k the real wavenumber, equation (6), with appropriate boundary conditions, has been the starting point for numerous studies of stability of the baroclinic velocity profile $\overline{U}(z)$ to small disturbances. Generally one determines a dispersion relation $c(k)$ for the waves and looks for roots with real k and complex $c = c_r + ic_i$. A root giving positive c_i indicates instability. Eady's (1949) analysis of the stability of a uniform shear flow with constant stratification is a particularly simple example. He discovered that this profile is unstable to waves longer than a critical wavelength with a maximum growth rate at some intermediate value. These unstable waves have phase velocity equal to the vertical average of the velocity of the basic state and are non-dispersive. Eady also found that neutral waves can exist for the linear profile and that these waves have a phase velocity somewhere between the surface and bottom values for the basic state. The level at which the phase velocity exactly cancels the underlying flow velocity is now known as the 'steering level'.

Green (1960) went several steps further and included β and velocity curvature in his analysis. His conclusion was that β acts to destabilize the flow at all wave-

lengths. Using physical arguments Bretherton (1966) rationalized this result and showed that all infinitesimal waves with a steering level within the fluid must be unstable. As Charney & Stern (1962) and Lin (1955, chap. 7) have pointed out, there is a close parallel between the problems of stability of baroclinic flows and of parallel homogeneous shear flow. The latter has shown (Lin 1955, p. 119) that a necessary condition for instability is that the curvature in the basic flow changes sign within the fluid. For continuously varying baroclinic flows this corresponds to $Q_y = \beta - (f^2 \overline{U}_z/N^2)_z$ vanishing between the top and bottom boundaries. The analogy between the two situations is most obvious when, for the baroclinic case, the density $\overline{\rho}(y, z)$ is constant on the two boundaries (i.e. $\overline{U}_z(z) = 0$ at $z = 0, -H$). Bretherton (1966) has shown how variation in $\overline{\rho}(y, z)$ on the boundaries can be thought of as sheets of potential vorticity along the boundaries which must be included in (6). For reasons which will be elaborated in §§3 and 4, we shall be interested here in the simpler situation in which

$$\overline{U}_z(z) = 0 \quad \text{at} \quad z = 0, -H. \tag{8}$$

In this case the only mechanism for balancing the creation of relative vorticity in (6) comes from cross-stream motion, which feels the variation in the slope of the isopycnals with depth. Green (1960, his §8*a*) points out that in such a case it may be possible to have instability in a deep fluid that bears no relation to the boundary and that the wave amplitude will be a maximum near the steering level. McIntyre (1972) has worked out such an example as a model of the polar night jet.

Pursuing the analogy with homogeneous shear flow somewhat further, it has also been pointed out that stability analyses of the above type are not strictly applicable to laboratory simulations (Watson 1962; Gaster 1962, 1965*a*, *b*). Here one generally introduces a disturbance to the flow with a real frequency and this grows *spatially* in the direction of wave propagation. In these situations one should choose k to be complex and $\omega = kc$ to be real in (7). Gaster (1962, 1965*a*, *b*) finds that, under certain conditions, a temporally growing perturbation can be related to a spatially growing one with the same real part of the wavenumber through a group-velocity transformation.

For the model we choose for a baroclinic flow, we find that this transformation does not hold: spatially growing waves are quite different in their properties. In fact, temporally growing waves are confined to long wavelengths while spatially growing ones are short with the dividing, critical wavelength corresponding to a neutral wave.

We believe that these spatially growing waves may have physical relevance under certain circumstances. A wave maker sitting on the bottom in a baroclinic flow and oscillating with real frequency ω will produce waves with this frequency which will propagate in the direction of their group velocity. Solutions to the dispersion relation, under certain conditions, will allow roots with an imaginary part of $k = k_r + ik_i$ with the appropriate sign, thus indicating spatial instability. As the frequency of generation decreases towards zero, the phase velocity of the waves will also tend towards zero. In the limit a steady situation will exist in which spatially growing, stationary waves exist in the 'downstream' (defined by

the group velocity) direction. Although one would have to resort to an initial-value problem to prove this rigorously, we believe that this may be an appropriate framework for considering the effects of such steady disturbances as bottom roughness (seamounts, ridges, etc.) on the stability of baroclinic flows. Here we shall not solve the full problems of response of the fluid to a wave maker or bottom relief; the basic assumption is made that in the limit of long times the disturbance with largest amplitude will be that given by the spatially growing normal mode with frequency tending to zero. This is a crucial assumption and we hope to be able to report progress on this aspect of the problem in the future.

Use of (7) in the vorticity equation (6) yields the vertical eigenvalue equation:

$$\frac{\partial}{\partial z}\left(\frac{f^2 F_z}{N^2}\right) = \left(k^2 - \frac{Q_y}{\overline{U}(z) - c}\right) F, \tag{9}$$

with the boundary condition $w = 0$ at $z = 0, -H$ determined from (4) and (8) to give

$$F_z = 0 \quad \text{at} \quad z = 0, -H. \tag{10}$$

If we multiply (9) by F^*, subtract from the result F times the conjugate, and then integrate over the depth using (10) we obtain a form of the Rayleigh stability criterion for flows with both k and c complex:

$$2\, k_r k_i \int_{-H}^{0} |F|^2 dz = c_i \int_{-H}^{0} \frac{Q_y |F|^2}{|\overline{U} - c|^2}\, dz. \tag{11}$$

From (11) we can see that the necessary condition for temporally growing waves ($k_i = 0, c_i \neq 0$) is that Q_y changes sign within the fluid. On the other hand spatially growing waves, in the limit of zero frequency ($c_i \to 0$), satisfy the relation

$$2k_r k_i \int_{-H}^{0} |F|^2 dz = \frac{Q_{yc} |F_c|^2}{\overline{U}_{zc}} \pi \operatorname{sgn}(\overline{U}_{zc}\, c_i), \tag{12}$$

with the subscript c indicating evaluation at the steering level, where

$$\overline{U}(z) = \overline{U}_c = 0.$$

Neutral waves ($k_i = 0$) are possible only if $Q_{yc} = 0$, i.e. if Q_y vanishes at the steering level. The sign of k_i depends upon the direction of approach of c_i to zero.

We also note that the depth-averaged or barotropic component of $\overline{U}(z)$ in (9) is equivalent to a negative real part for the phase velocity. In what follows we shall investigate the dependence of the complex eigenvalue k on the complex phase velocity c by taking

$$\int_{-H}^{0} \overline{U}(z)\, dz = 0$$

and varying c_r and c_i independently. Results for $\omega \to 0$ can be recovered by allowing $c_i \to 0$ and taking c_r equal to minus the barotropic mean flow component.

Using the momentum equations, the density equation (4) and continuity it is possible to derive an energy equation in the usual way as $\omega \to 0$. Averaging over a period in time, this is

$$\overline{U}(z) \frac{\partial}{\partial x}\left[\overline{\frac{u^2 + v^2}{2} + \frac{g^2}{\rho_0 N^2} \frac{\rho^2}{2}}\right] = -\frac{gf}{N^2} \overline{U}_z \overline{v\rho} \tag{13}$$

and relates changes in the perturbation energy to the energy flux in the wave and conversion from the store of potential energy in the basic flow.

We shall also be interested in the direction of energy propagation in the growing waves. This is given by the real part of the group velocity $c_g = \partial\omega/\partial k$. Writing $\omega = ck$ and taking the limit of zero frequency, it can be shown that

$$\operatorname{Re} c_g = c_r + \frac{1}{2}\frac{\partial|k|^2/\partial c_r}{|\partial k/\partial c_r|^2} \quad \text{as} \quad \omega \to 0, \tag{14}$$

where $c_r = \operatorname{Re} c$.

3. Numerical results

By numerical integration of (9) satisfying (10) at $z = 0$ we have determined the eigenvalue k for various c's by adjusting k until the bottom boundary condition is satisfied. Because the equation must be dealt with numerically it is necessary to specify the shear-flow profile. Our interest is in looking at the effects of interior potential-vorticity gradients on the instability problem. As Bretherton (1966) shows, lateral density variations at the boundaries are equivalent to concentrated sheets of potential vorticity; if these gradients are of the appropriate sign, further changes in the sign of Q_z can be concentrated at the boundary and complicate the analysis. We shall remove these effects by restricting our profiles to satisfy (8) so that the density is uniform on the boundaries. A natural choice for such a profile is the lowest vertical mode of oscillation of the resting fluid (the so-called 'first baroclinic mode' is given by the lowest eigenfunction of (9) and (10) with $Q_y \equiv 0$ and $F(z) = U(z)$, k being the eigenvalue). This choice was motivated by the observations we present in §4.

Two forms of density stratification are considered:

(i) $N(z)/f = 25{\cdot}5$, where $\overline{U}(z) = A_1 \cos \pi z/H$;

(ii) $N(z)/f = 112 \exp(z/1800)$,

where $\overline{U}(z) = A_2[Y_0(\lambda)J_1(\lambda e^{z/1800}) - J_0(\lambda)Y_1(\lambda e^{z/1800})]$, $\lambda = 3{\cdot}227$.

In both cases the bottom depth has been chosen to be $H = 5500$ m and the Brunt–Väisälä frequencies were chosen such that

$$\int_{-H}^{0} N dz/H = 1 \text{ cycle per hour}, \quad f = 1/25{\cdot}5 \text{ cycle per hour},$$

values that are typical of the mid-latitude North Atlantic. We have taken

$$\int_{-H}^{0} \overline{U}^2(z)\, dz/H = 1, \quad \int_{-H}^{0} \overline{U}(z)\, dz = 0$$

so that $\overline{U}(z)$ is normalized (this defines A_1 and A_2) and has zero integrated transport. From the form of Q_y and $\overline{U} - c$ in (9) it can be seen that changes in the amplitude of $\overline{U}(z)$ are equivalent to inverse changes in c while changes in the barotropic component of $\overline{U}(z)$ are equivalent to negative changes in c_r. We therefore consider c also to be normalized by the root-mean-square amplitude of the mean flow and, in the zero-frequency limit, c_r to be equal to minus the depth-integrated transport (also normalized).

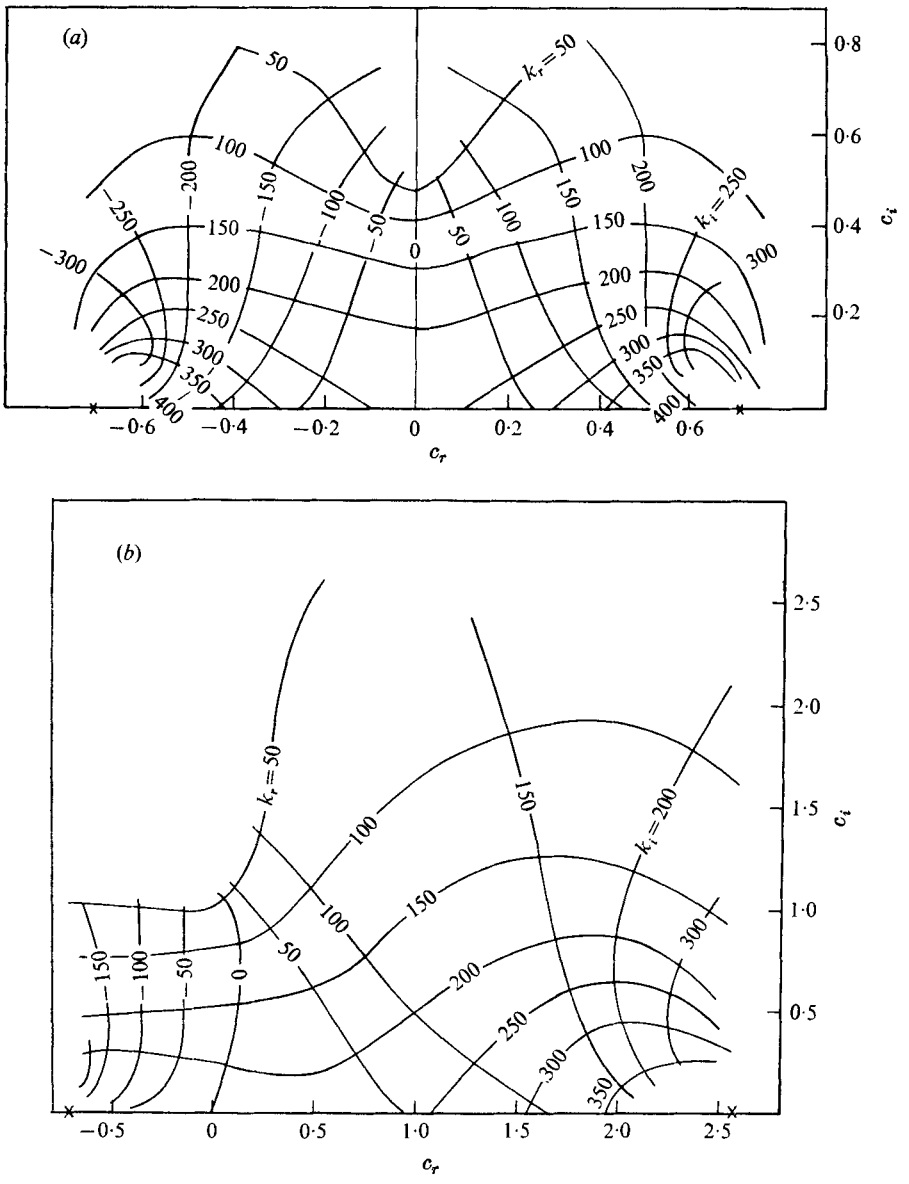

FIGURE 1. Contours of the real and imaginary parts of k ($\mathrm{km}^{-1} \times 10^4$) in the complex c plane for (*a*) constant and (*b*) exponential Brunt–Väisälä frequency. The crosses indicated singularities where c_r equals either the bottom or the surface current.

Contours of k_r and k_i in the complex c plane are presented in figures 1 (*a*) and (*b*) for the two cases. Results are only given for $c_i > 0$, but from the form of (9) it can be seen that $F(z, k, c) = F^*(z; k^*, c^*)$, so that the lower half-plane mirrors the upper one with the only change being that k_i changes sign. It can also be seen from (9) that $F(z; k, c) = F(z; -k, c)$, so that for any c two solutions exist. Except at isolated singularities contours of k_r are orthogonal to those of k_i, indicating that k is an analytic function of c.

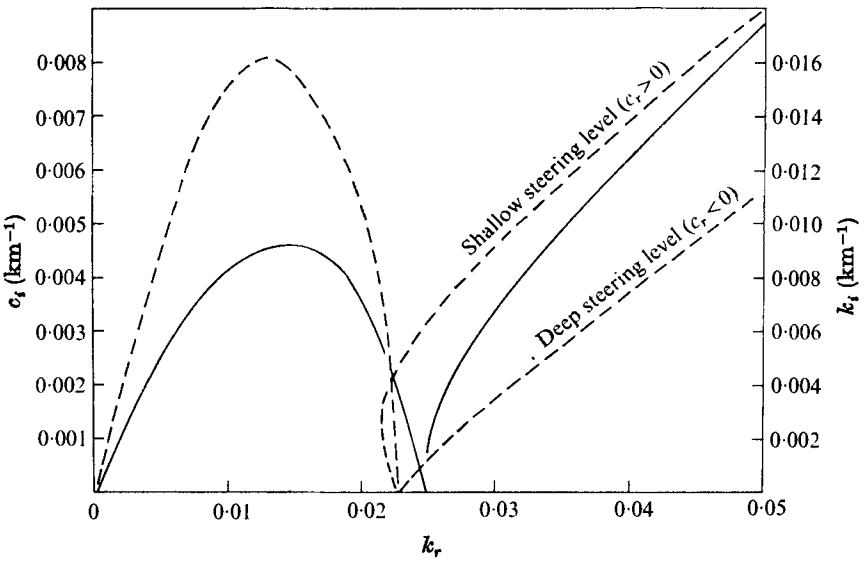

FIGURE 2. Temporal and spatial growth rates as a function of k_r. ——, constant N; – – –, exponential N.

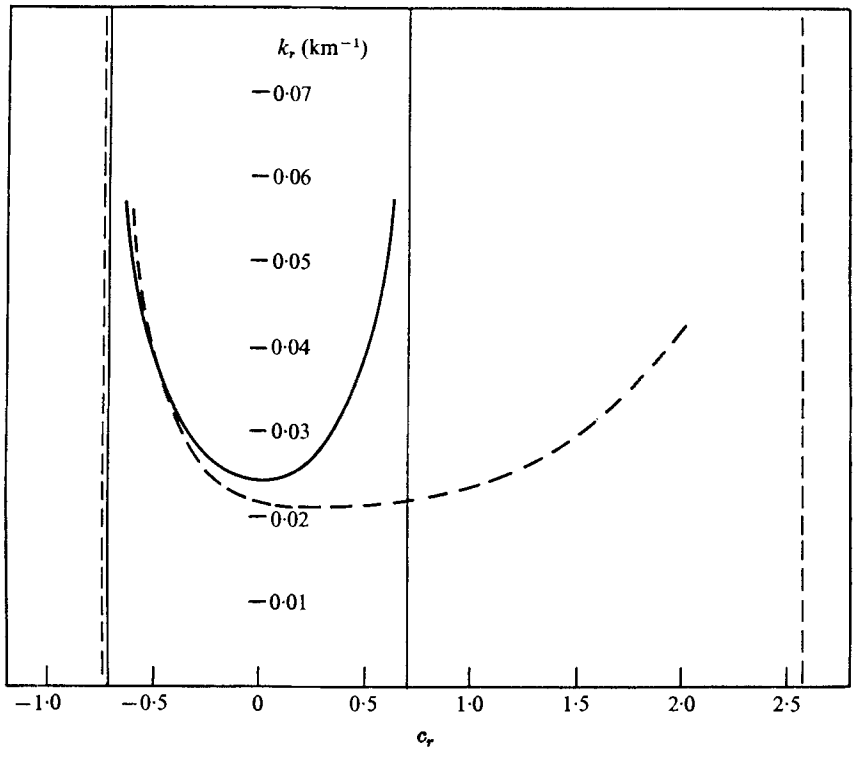

FIGURE 3. The real part of the wavenumber k_r plotted against c_r for spatially growing waves with $c_i = -0{\cdot}01$. Vertical lines indicate values of c_r for which the steering level is at a boundary. ——, constant N; - - -, exponential N.

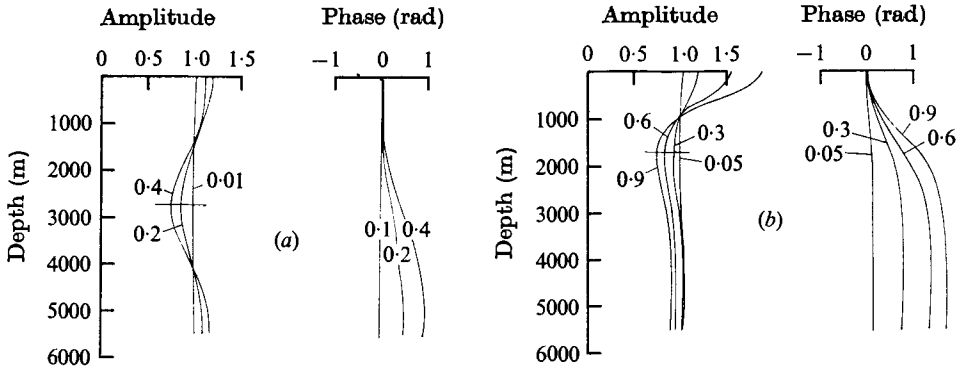

FIGURE 4. Modal amplitudes and phases for $c_r = 0$ with (*a*) constant and (*b*) exponential Brunt–Väisälä frequency. For (*a*) the waves are purely temporally growing while for (*b*) there is a slight spatial component (see figure 1). The thin horizontal line indicates the steering level.

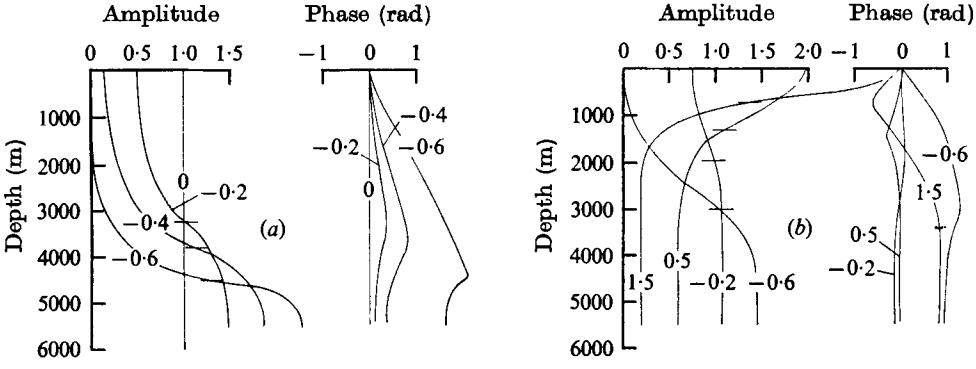

FIGURE 5. Modal amplitudes and phases for various c_r and $c_i = -0{\cdot}01$ with (*a*) constant and (*b*) exponential Brunt–Väisälä frequency. These waves are spatially growing and the thin horizontal lines indicate steering levels.

The case of constant stratification is symmetric about the mid-depth, leading to symmetry about $c_r = 0$. Note also that $c_r = 0$ corresponds to $k_i = 0$ and temporally growing waves, as in the Eady (1949) model. The temporal growth rate is kc_i and is presented in figure 2. The quantity kc_i approaches zero at two points in figure 1 (*a*): as $c_i \to 0{\cdot}52$ where $k \simeq 0$ and as $c_i \to 0$ where $k \simeq 0{\cdot}25$. The latter point is the high wavenumber cut-off characteristic of Eady-type models without β.

The axis $c_i = 0$ gives rise to a regular singular point in (9) and, as was shown in §2, equation (12), the result obtained depends on the direction of approach (i.e. on whether $c_i \to 0^+$ or 0^-). This axis also corresponds to the case of purely spatial growth and we note the remarkable result that k_r is now bounded by a low wavenumber cut-off where $c_r = 0$. As c_r increases from this point so does k_r (this is shown in figure 3). In fact $k_r \to \pm\infty$ as $c_r \to U(0)$ or $c_r \to U(-H)$ when the steering level is at one of the boundaries. The spatial growth rate $|k_i|$ increases in a similar fashion and this is shown in figure 2 along with the temporal growth rates.

We arrive at the important conclusion that long waves are temporally

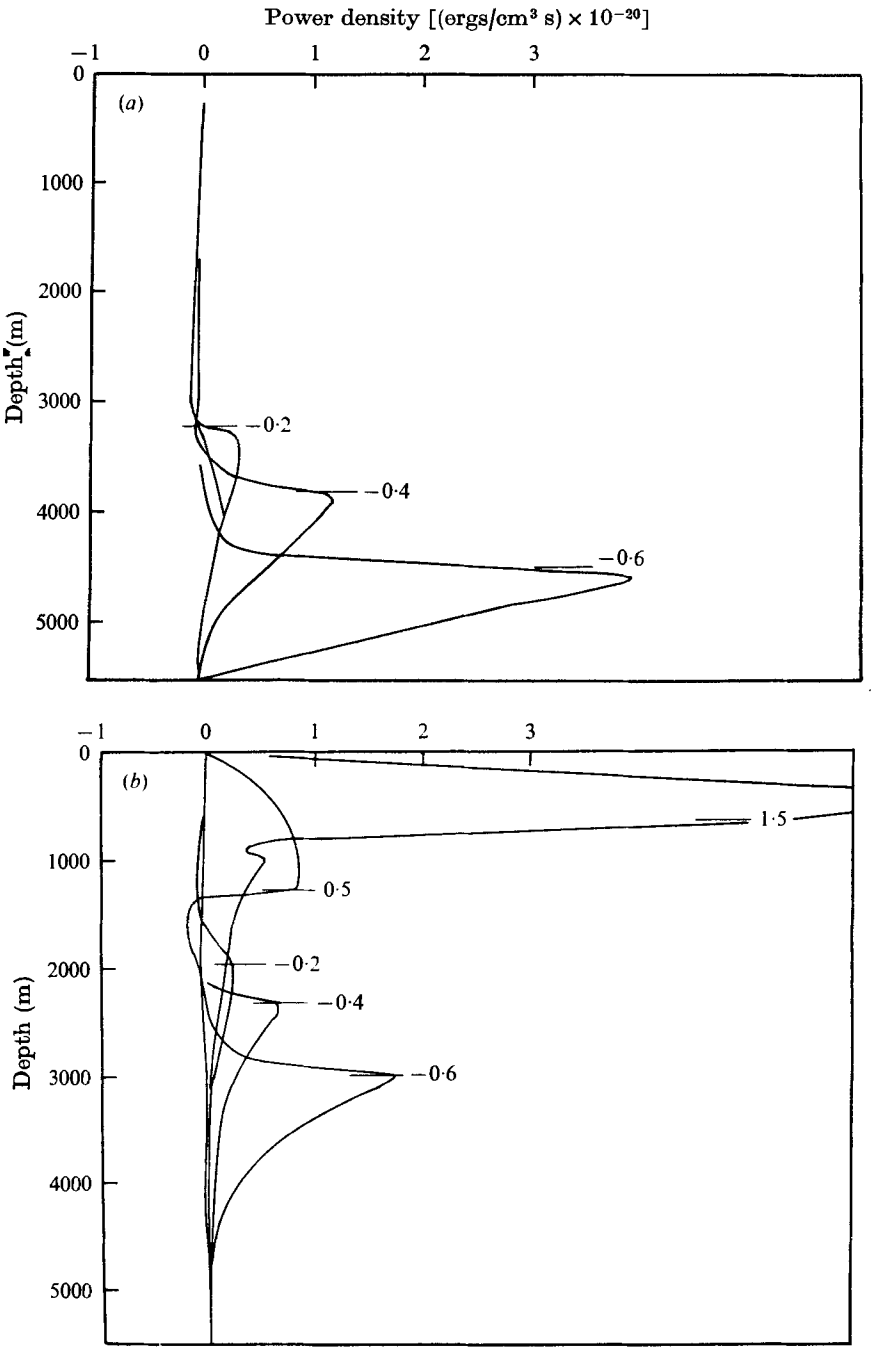

FIGURE 6. Reynolds stresses as a function of depth for (*a*) constant and (*b*) exponential Brunt–Väisälä frequency. The thin horizontal lines indicate steering levels.

unstable while short waves are spatially unstable. There exists a critical wavenumber for which $Q_{yc} = 0$ and a neutral wave can exist.

The exponentially stratified model gives similar results except that symmetry about $c_r = 0$ disappears (see figure 1*b*). The temporally growing waves with $k_i = 0$ are no longer non-dispersive and c is a function of k_r. However, there remains a high wavenumber cut-off as is illustrated in figure 2. Similar results to case (i) are also obtained for the spatial growth (figure 2) and the dependence of k_r on c_r (figure 3).

From equation (14) for the group velocity and figures 2 and 3 for the dependence of k on c_r, it can be easily seen that the sign of Re c_g is the same as the sign of c_r. Spatially growing waves are therefore those found as $c_i \to 0^-$, so that sgn $k_i = -\text{sgn}(\text{Re}\, c_g)$. Modal amplitudes for the disturbance pressure are presented in figure 4 for the case of temporal growth ($c_r = 0$) and in figure 5 for spatial growth ($c_i = -0{\cdot}01$).

The constant-N model gives temporally growing waves with shape similar to cos $2\pi z/H$ while the exponential stratification concentrates variation near the surface, where there exists the store of potential energy (figure 4). The spatially growing modes are substantially different (figure 5). They undergo rapid changes in the neighbourhood of their steering level, where (9) has a singularity of the form $F(z) \sim (z - z_c)\log(z - z_c)$ for $c_i = 0$ as $z \to z_c$. Above and below this point variations are much less rapid. It is apparent that there are two height scales for this problem, one given by the depth of the steering level and the other given by a Rossby deformation scale f/Nk_r.

We have also computed the Reynolds-stress term in the energy conversion (13) for the spatially growing perturbations. This is presented as a function of depth in figure 6 for the two cases. In general the stress reaches a maximum close to the steering level. When this is deep (i.e. below the depth at which $Q_y(z) = 0$) the maximum appears to be just below the steering level. Taking into account the signs of $\overline{U}(z)$ and Re c_g, there seems to be a small region above the steering level in which energy is transferred from the perturbation field to the mean flow. This is more than compensated for by transfer in the opposite direction below the steering level.

4. Discussion and observations

In the Mid-Ocean Dynamics Experiment (MODE-I), effects of small-scale topography were studied in the field with an electromagnetic velocity profiler (EMVP) by Tom Sanford [see Leaman & Sanford (1975) and Sanford (1976) for a discussion of the instrument and other results] and with neutrally buoyant floats, current meters and a conductivity, temperature *vs.* depth sensor (CTD) by the Institute of Oceanographic Sciences. This paper was inspired by the data collected by these groups; a more complete description will be given by them in the future.

Figure 7 shows the region of concentrated study and the positions of pairs of velocity profiles. It has been shown by Leaman & Sanford (1975) that the small-scale vertical structure is dominated by inertial motion (period $\simeq$ 25·5 h).

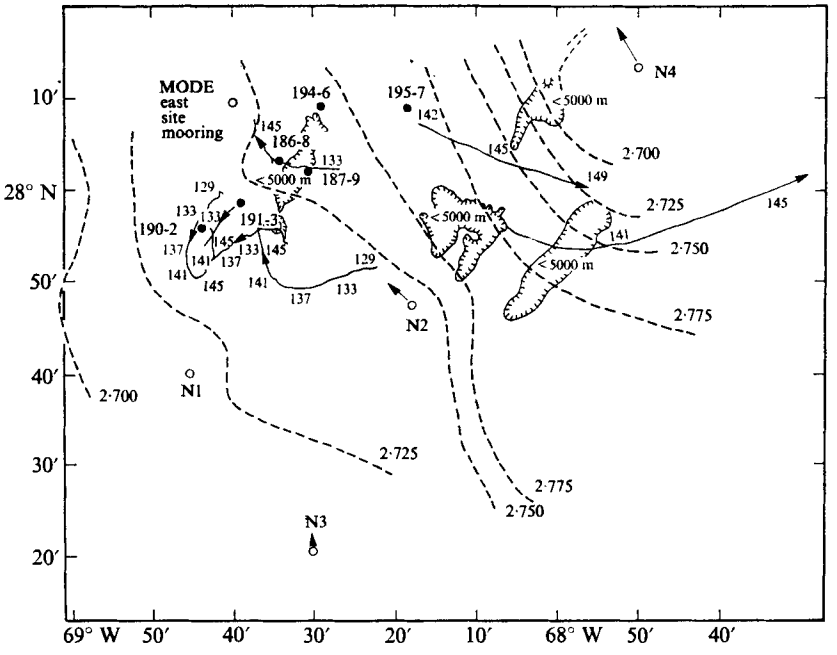

FIGURE 7. Bathymetric chart of the area in MODE-I which was intensively studied with velocity profiling (numbered solid dots), density measurements (dashed lines are temperature contours) and current measurements (solid lines with arrows).

Averaging two profiles obtained half an inertial period apart at one location is a crude filter. This has been done for the six pairs and, after a further smoothing over 50 m in the vertical, the east and north components are presented in figure 8. It is important to realize that this indirect method of measuring velocity senses only the velocity relative to an undetermined reference value which varies from location to location and slowly with time.

We wish to note two striking features of these average profiles. First, to the west over the abyssal plain (profile 190–2), there is little structure to the east–west component but the north–south component is dominated by considerable shear in the region of the main thermocline. Profiles similar to this were obtained elsewhere over the smooth abyssal plain and seem to be a property of the low-mode character of the mesoscale eddy field in the area, at least away from the rough bottom region. This main thermocline shear lessens as one moves a short distance east (profile 191–3) and into the seamount area.

The second feature we should like to emphasize is the appearance of a mid-water maximum in current speed at about 2700 dbar to the north and north-east of a small seamount (profiles 194–6 and 195–7). This strong current is also revealed in the neutrally buoyant float tracks of John Swallow, which were taken at more or less the same time as the velocity profiles. Figure 7 shows float tracks at roughly 3000 dbar. Also shown are averaged current vectors at this level from moored current meters. We note the strong south-east current in the east and the rather small horizontal scale indicated by the floats and current meters. It

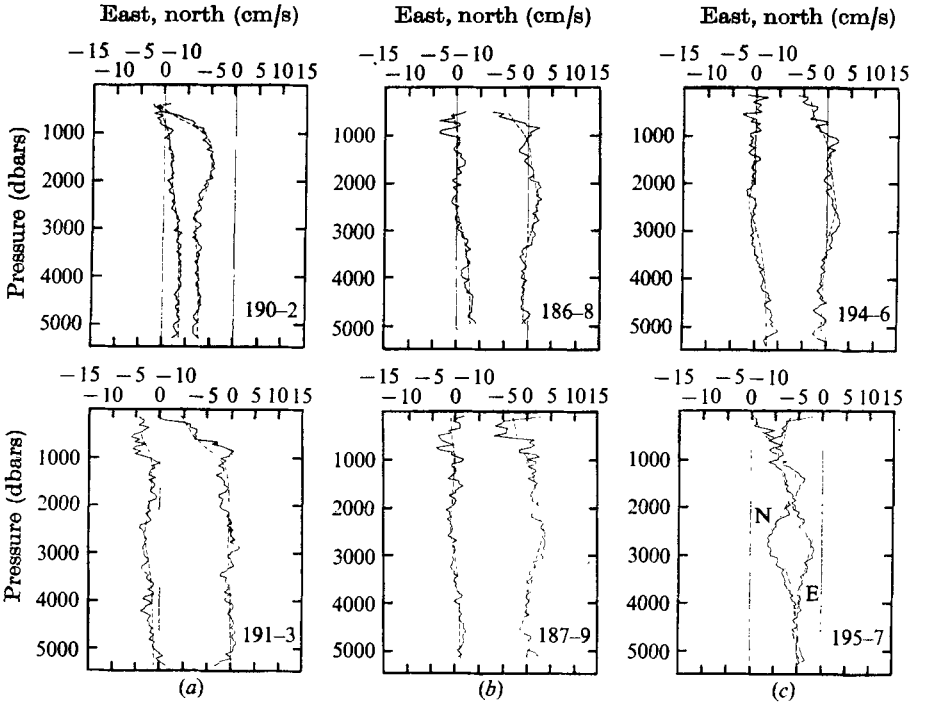

FIGURE 8. Velocity profiles observed at the locations shown in figure 7. (*a*) Smooth. (*b*) Seamount. (*c*) Between seamounts. Solid lines are the average of pairs of profiles taken half an inertial period apart in time and further smoothed over 50 m in the vertical. The zero level was not measured and has been established by the least-squares-fit procedure. Dashed curves are least-squares fits to the unstable wave plus mean flow according to (18).

appears that this current is approximately geostrophic. Also drawn on figure 7 are 2600 dbar temperature deviations; these contours are almost parallel to the float tracks.

We apparently have evidence, therefore, of a disturbance to the eddy flow in the region of rough topography that has relatively small vertical and horizontal scales. In order to tie this in with the larger mesoscale, we present in figure 9 a concurrent map of the temperature field interpolated from moored instruments at a depth of 418 m with current vectors superimposed. Note the strong north–south lineations over the region of interest, which is roughly 100 km east of the central mooring (no. 1). This eddy pattern propagated west at abour 3 cm/s (Scarlet, personal communication; Richman, Hogg & Wunsch 1976). It has been interpreted in terms of a superposition of two barotropic and two first baroclinic mode Rossby waves by McWilliams & Flierl (1976). Sanford's EMVP profiles away from the rough topography are consistent with this explanation: over 95 % of the baroclinic energy in the average of 5 profiles taken over 2 days at the central mooring (no. 1 in figure 9) is contained in the first baroclinic mode. We shall interpret the observations in the seamount area as being evidence of spatial instability of the MODE-I eddy.

The low-mode character of the eddy is our principal motivation for choosing

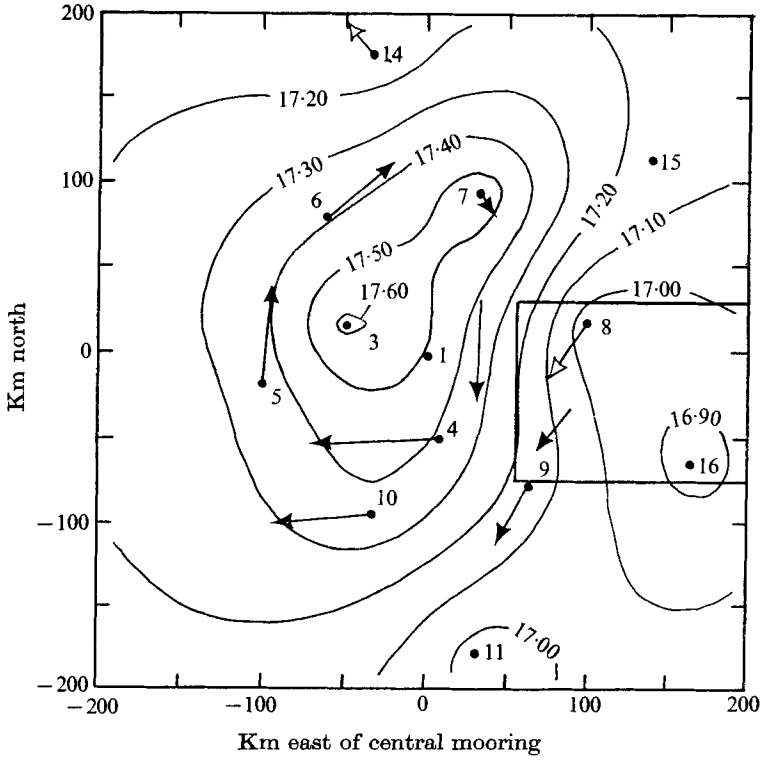

FIGURE 9. A temperature map at a depth of roughly 400 m with velocity vectors superimposed for the time period corresponding to the other measurements. The box on the right is the region expanded in figure 7.

the first baroclinic mode as the mean flow. It should be noted, however, that the higher-order vertical structure may be important. McWilliams & Flierl (1976) have pointed out that the shear near the surface is generally stronger than that predicted by the first baroclinic mode (in which the shear vanishes at horizontal boundaries). They further show that a surface-concentrated mean zonal current can modify the first baroclinic mode in the desired fashion. We also note that the potential-vorticity gradient Q_y depends on a stratification-modified curvature in the basic flow: even though the profile itself might be dominated by the first mode, this curvature brings in a strong weighting of the higher modes and may not be so dominated. We have neglected a number of other known properties of the 'mean' flow, such as its slow westerly propagation and lateral variations, so that inclusion of higher-order vertical structure would seem to be inconsistent.

Assuming that the profiles from the seamount area are dominated by a basic flow and the spatially growing disturbance, we can write the measured horizontal velocity $\mathbf{u}_m(z;x,y)$ as

$$\mathbf{u}_m(z;x,y) = \mathbf{A}_0(x,y) + \mathbf{A}_1(x,y)\,\overline{U}(z) + \mathbf{A}_2^*(x,y)\,(-p_y, p_x) + \boldsymbol{\epsilon}(z;x,y), \tag{15}$$

where

$$\begin{aligned} p(x,y,z) &= P\,\mathrm{Re}\{|F(z)|\exp[i(kx+ly+\phi(z)+\psi)]\} \\ &= P|F(z)|\exp(-k_i x - l_i y)\cos(k_r x + l_r y + \phi(z) + \psi), \end{aligned} \tag{16}$$

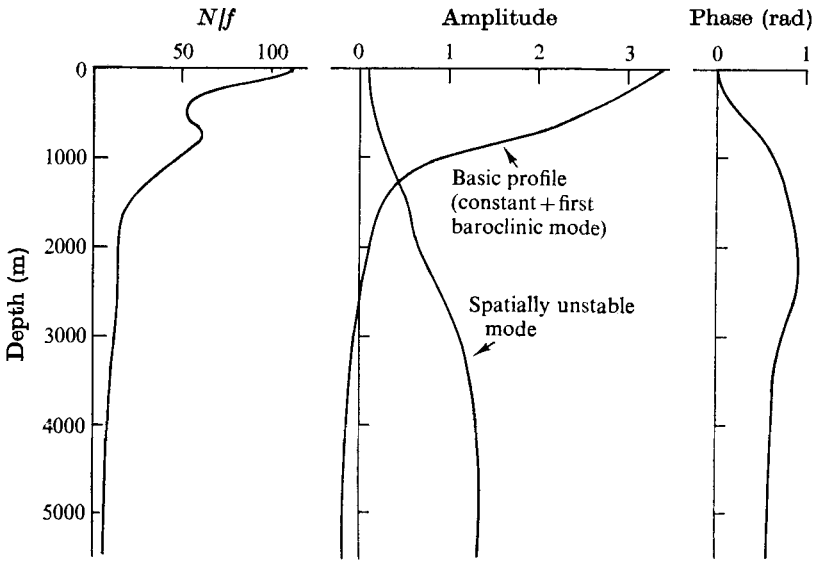

FIGURE 10. An average Brunt–Väisälä profile from MODE-I (Bryden & Millard 1973) with the corresponding first baroclinic mode offset by $c_r = -0{\cdot}42$ to give a steering level of about 2500 dbar. Also shown are the amplitude and phase of the spatially growing disturbance.

with $\phi(z)$ the argument of the complex normalized amplitude $F(z)$, P the actual pressure amplitude and ψ a constant phase angle. By including the y wavenumber component l, we permit an arbitrary orientation of the plane-wave disturbance. $\mathbf{A}_0(x, y)$ is the reference velocity in the profiles. If we now define amplitudes and angles according to

$$l_r = L\cos\alpha, \quad l_i = L\sin\alpha, \quad k_r = K\cos\beta, \quad k_i = K\sin\beta, \tag{17}$$

then (15) can be rewritten as

$$\mathbf{u}_m(z;x,y) = \mathbf{A}_0(x,y) + \mathbf{A}_1(x,y)\,\mathbf{U}(z) + \mathbf{A}_2(x,y)\,|F(z)|\cos\phi(z) + \mathbf{A}_3(x,y)\,|F(z)|\sin\phi(z) + \boldsymbol{\epsilon}(z;x,y) \tag{18}$$

and

$$\mathbf{A}_2(x,y) = P\exp(-k_i x - l_i y)\,[\sin(k_r x + l_r y + \alpha + \psi), \sin(k_r x + l_r y + \beta + \psi)],$$
$$\mathbf{A}_3(x,y) = P\exp(-k_i x - l_i y)\,[\cos(k_r x + l_r y + \alpha + \psi), \cos(k_r x + l_r y + \beta + \psi)]. \tag{19}$$

We can see then that knowledge of $\mathbf{A}_2(x, y)$ and $\mathbf{A}_3(x, y)$ permits us to determine both the growth rate and the wavenumber. The ratios of the amplitude components give

$$k_r x + l_r y + \psi = \tan^{-1}\left(\frac{A_{2x}}{A_{3x}}\right) - \alpha = \tan^{-1}\left(\frac{A_{2y}}{A_{3y}}\right) - \beta, \tag{20}$$

while the sums of their squares yield

$$k_i x + l_i y = \log_e P + \tfrac{1}{2}\log_e[A_{2x}^2 + A_{3x}^2] = \log_e P + \tfrac{1}{2}\log_e[A_{2y}^2 + A_{3y}^2]. \tag{21}$$

In order to calculate $F(z)$ it is necessary to know the barotropic part of $\overline{U}(z)$. From figures 4 and 5 we see that the shear is greatest in the neighbourhood of the

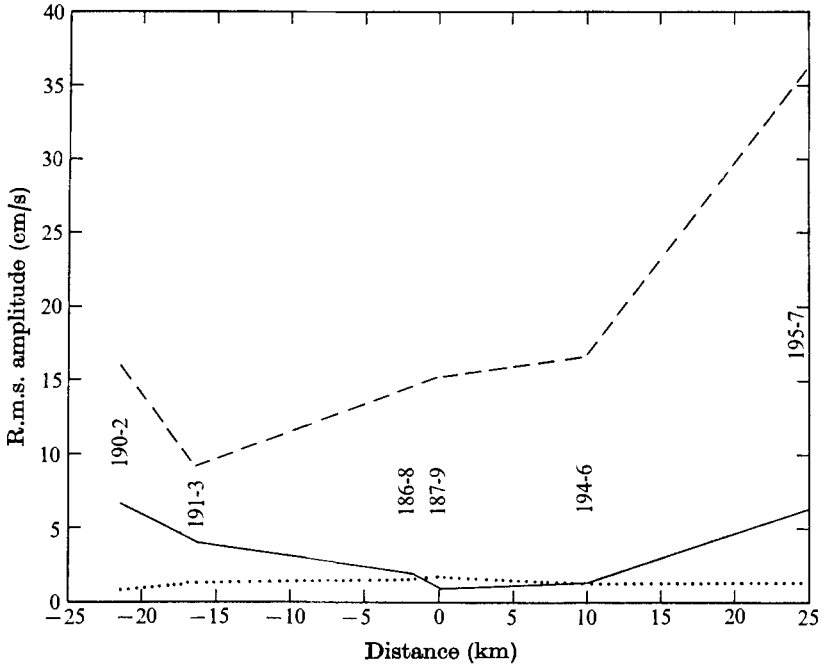

FIGURE 11. Amplitudes of the unstable wave, mean flow and residue determined from the least-squares procedure as a function of position. ——, basic flow; - - -, wave; · · ·, residue.

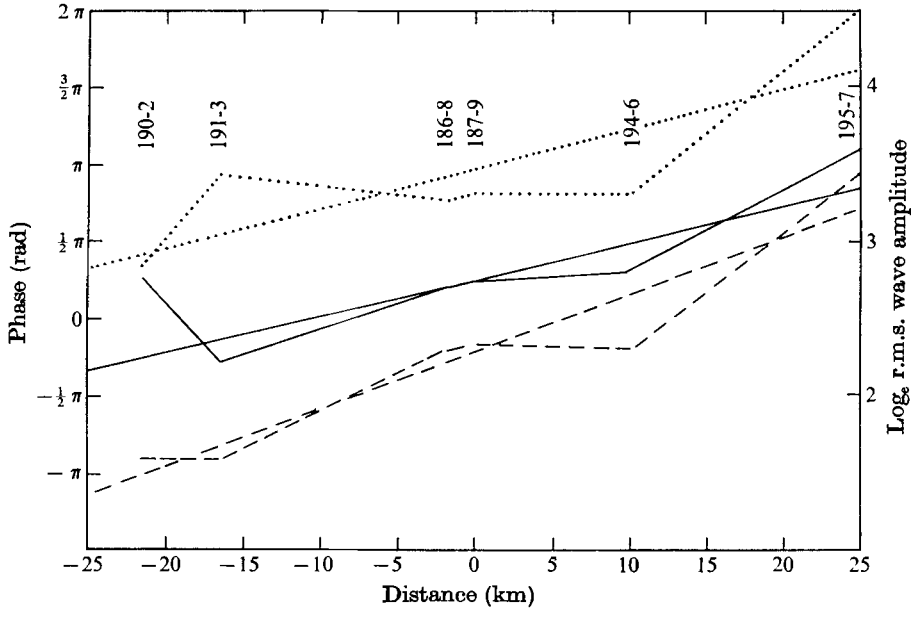

FIGURE 12. Phase and logarithm of the wave amplitude as a function of distance. · · ·, east-component phase; - - -, north-component phase; ——, r.m.s. wave amplitude.

steering level. From figure 8 we choose this depth to be 2500 dbars (1 dbar $\approx$ 1 m). An average Brunt–Väisälä profile for the MODE-I experiment has been determined by Bryden & Millard (1973): its form after some vertical smoothing is shown in figure 10 along with the corresponding first baroclinic mode and the amplitude and phase of the spatially growing wave with $c_i \to 0^-$ and appropriate c_r. The wavenumber of the wave is $k = (0{\cdot}0393 + 0{\cdot}0095i)\,\mathrm{km}^{-1}$, giving a wavelength of 160 km and an e-folding length of 105 km. We shall attempt to compare these numbers with estimates obtained from the observations through fitting (19), in a least-squares sense, to the profiles and using (20) and (21).

Each profile pair in figure 8 was decomposed according to (19) by minimizing the depth-integrated residual $\epsilon(z; x, y)$ in a least-squares manner. Results are given in figures 10–12 and confirm what the eye can see. The amplitude of the mean flow decreases as one moves east into the seamount area while the amplitude of both the wave and the residual increase. We note also that (14) predicts a group velocity in the opposite direction to the surface flow and, therefore, to the north. From (14) and figures 2 and 3 we estimate the group speed to be of order 5 cm/s or 5 km/day: large enough for the perturbation to grow and propagate a significant amount on the time scale characteristic of the eddy (period of about 250 days, McWilliams & Flierl 1976). It seems plausible that the disturbance is actually triggered by the small bottom relief in the area (the seamounts have lengths of about 10 km and heights of about 700 m).

In figure 12 we show the variation in the arc tangents of the amplitude ratios according to (20). The stations lay in an almost straight line running slightly north of east, so that we are able to estimate the wavenumber component only along this line. There is, as well, an ambiguity of 2π in the definition of the angle so determined; this has been arbitrarily removed where there is doubt, by forcing the phase angle to increase towards the east. From the east-component fits we find that $k_r = 0{\cdot}082\ \mathrm{km}^{-1}$ (wavelength of 76 km) while the north components give $k_r = 0{\cdot}116\ \mathrm{km}^{-1}$ (wavelength of 54 km). Variation of the amplitudes according to (21) gives a growth rate $k_i = 0{\cdot}021\ \mathrm{km}^{-1}$ (e-folding scale = 48 km) for the averaged east and north components.

These estimates exceed the predicted values by a factor of more than 2. We note that the theoretical curves predict that the wavenumber is a strong function of c_r for a deep steering level and an improper choice of this quantity may account for some of the discrepancy. However, we have made a large number of gross approximations and, because k has no upper bound in this model without dissipation, it seems plausible that a more general form of spatial instability could account better for the observations.

Peter Saunders and Jim Luyten have profiled horizontal velocity in the neighbourhood of the Gulf Stream using an acoustically tracked, negatively buoyant device (Saunders & Luyten 1976). Figure 13 shows two five-day average profiles, one in the Gulf Stream and the other just north of the Gulf Stream. Within the stream, flow is dominated once again by a low-order structure with strong shears accompanying the strong density gradient of the main thermocline. The profile to the north, however, is decidedly different and is strikingly similar in shape to the rough-topography profiles in MODE-I. Additional evidence from a current-

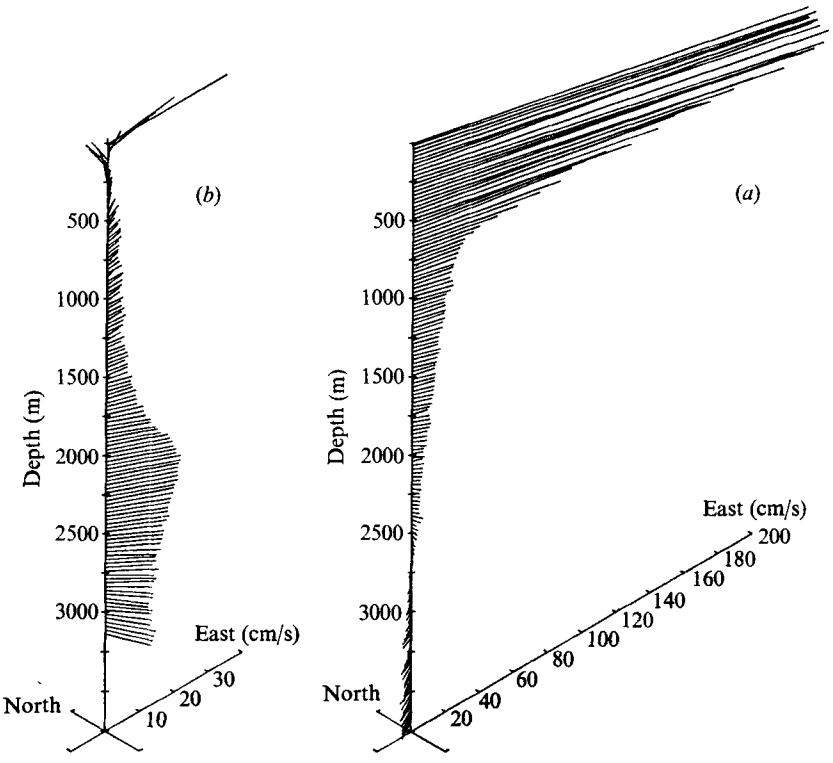

FIGURE 13. Velocity profiles (*a*) in and (*b*) near the Gulf Stream obtained by Saunders & Luyten (1976).

meter array (Luyten 1976) indicates that the deep motions beneath the stream are of small scale (< 50 km) and weak functions of depth near the bottom; both these features are characteristics of spatially growing modes. Although the Gulf Stream is a far more complicated system than that we have treated, it seems plausible that it may become spatially unstable after leaving the coast at Cape Hatteras.

This study was stimulated by Tom Sanford's observations: I thank him for continued encouragement, many discussions and permission to use his data. John Gould originally pointed out to me the lineations of the temperature field near 3000 m depth: I am grateful to him and John Swallow for permission to use their current meter vectors, float tracks and temperatures. Michael McIntyre found a crucial error in an earlier version of this paper which led me to discover that the waves had a complex wavenumber and were not neutral as I had first concluded. I am grateful, as well, to Francis Bretherton for discussions on this point and to the referees for comments which clarified the presentation. The work has been supported by the Office of Naval Research through Contract N00014-74-C-0262 NR 083-004 to the Woods Hole Oceanographic Institution. This is contribution no. 3605 of the Woods Hole Oceanographic Institution and contribution no. 43 of the Mid-Ocean Dynamics Experiment.

REFERENCES

BRETHERTON, F. P. 1966 Critical layer instability in baroclinic flows. *Quart. J. Roy. Met. Soc.* **92**, 325–334.

BRYDEN, H. & MILLARD, R. 1973 Spatially-averaged MODE-I CTD stations. *MODE Hot Line News*, **43**.

CHARNEY, J. G. 1947 The dynamics of long waves in a baroclinic westerly current. *J. Met.* **4**, 135–163.

CHARNEY, J. G. & STERN, M. E. 1962 On the stability of internal baroclinic jets in a rotating atmosphere. *J. Atmos. Sci.* **19**, 159–172.

EADY, E. T. 1949 Long waves and cyclone waves. *Tellus*, **1**, 33–52.

GASTER, M. 1962 A note on a relation between temporally increasing and spatially increasing disturbances in hydrodynamic stability. *J. Fluid Mech.* **14**, 222–224.

GASTER, M. 1965*a* The role of spatially growing waves in the theory of hydrodynamic stability. *Prog. Aero. Sci.* **6**, 251–270.

GASTER, M. 1965*b* On the generation of spatially growing waves in a boundary layer. *J. Fluid Mech.* **22**, 433–441.

GILL, A. E., GREEN, J. S. A. & SIMMONS, A. J. 1974 Energy partition in the large-scale ocean circulation and the production of mid-ocean eddies. *Deep-Sea Res.* **21**, 499–528.

GREEN, J. S. A. 1960 A problem in baroclinic stability. *Quart. J. Roy. Met. Soc.* **26**, 157–185.

LEAMAN, K. D. & SANFORD, T. B. 1975 Vertical energy propagation of inertial waves: a vector spectral analysis of velocity profiles. *J. Geophys. Res.* **80**, 1975–1980.

LIGHTHILL, M. J. 1967 On waves generated in dispersive systems by travelling forcing effects, with applications to the dynamics of rotating fluids. *J. Fluid Mech.* **27**, 725–752.

LIN, C. C. 1955 *The Theory of Hydrodynamic Stability*. Cambridge University Press.

LUYTEN, J. R. 1976 Scales of motion in the deep Gulf Stream and across the Continental Rise. To be published.

MCINTYRE, M. E. 1972 Baroclinic instability of an idealized model of the polar night jet. *Quart. J. Roy. Met. Soc.* **98**, 165–174.

MCWILLIAMS, J. C. & FLIERL, G. R. 1976 Optimal quasigeostrophic wave analysis of MODE array data. *Deep-Sea Res.* **23**, 285–300.

RICHMAN, J., HOGG, N. G. & WUNSCH, C. 1976 Analysis of MODE-I moored temperature observations. In preparation.

SANFORD, T. B. 1976 Observations of the vertical structure of internal waves. *J. Geophys. Res.* **80**, 3861–3871.

SAUNDERS, P. & LUYTEN, J. 1976 Velocity profiles in and near the Gulf Stream. In preparation.

WATSON, J. 1962 On spatially-growing finite disturbances in plane Poiseuille flow. *J. Fluid Mech.* **14**, 211–221.